Available online at www.eccomasproceedia.org
Eccomas Proceedia SMART (2023) 1497-1506

ECCOMAS
Proceedia

X ECCOMAS Thematic Conference on Smart Structures and Materials
SMART 2023
D.A. Saravanos, A. Benjeddou, N. Chrysochoidis and T. Theodosiou (Eds)

A NUMERICAL TOOL FOR THE ANALYSIS OF THE THERMOMECHANICAL BEHAVIOR OF CAVITY METAMATERIALS BASED ON THE BOUNDARY ELEMENT METHOD

DIMITRIOS C. RODOPOULOS[†] AND NIKOLAOS KARATHANASOPOULOS[*†]

[*]Tandon School of Engineering
New York University
New York, United States
e-mail: n.karathanasopoulos@nyu.edu

[†] Department of Mechanical Engineering
New York University Abu Dhabi
Abu Dhabi, United Arab Emirates
e-mail: d.rodopoulos@nyu.edu

Abstract. Recently, progress in additive manufacturing has led to a new class of artificial materials, named as metamaterials, with mechanical attributes that cannot be commonly found in natural materials. In the present work, a numerical tool for the calculation of the thermomechanical effective properties of metamaterials with inner cavities following variable topologies is developed. The formulation is based on the Galerkin Boundary Element Method for linear thermoelasticity. Thereupon, the effective thermal conductivity and elastic properties of a wide range of metamaterial topologies are computed through the mere discretization of the domain boundaries. The numerical tool is developed and implemented for the effective property calculation in examples of cavity metamaterials.

Key words: Metamaterials, Galerkin Boundary Element Method, Thermoelasticity, design and optimization

1 INTRODUCTION

Progress in additive manufacturing has led to the design of a new class of advanced materials with complex architected inner designs, named as metamaterials [1, 2, 3]. These materials are characterized by mechanical properties that are commonly cannot be found in natural materials. In the last decades, a wide number of metamaterial architectures has been developed and employed in mechanical, aerospace, automotive and medical engineering applications [4, 5]. Therefore, the design and optimization of these materials is significant topic of active research.

In order to obtain optimal metamaterial geometries, an accurate method for the effective property computation is required. Such, methods are numerical methods, mostly Finite Element Method, machine learning modeling and analytical methods [6, 7].

Peer-review under responsibility of the organizing committee of SMART 2023.
doi: 10.7712/150123.9921.445020

The Boundary Element Method is a well-known numerical method based on boundary integral equations that requires surface only discretization ([8, 9]). The present work deals with the thermomechanical analysis of cavity metamaterials. The geometry of a cavity metamaterial can is readily generated through its parametric form. As such, the surface mesh can be generated by a simple code, without the need of a mesh generator. Also, the Boundary Element Method is characterized by accurate flux evaluations, as the field fluxes are calculated on boundary mesh nodes solving the final algebraic system. Therefore, there is no need of post process differentiation of shape functions. These advantages make the Boundary Element Method a reference numerical tool for the design of metamaterials.

The purpose of this work is the development and proposition of a numerical tool based on Boundary Element Method for the effective properties computation of a cavity metamaterial, performing thermoelastic analysis. The paper is organized as follows: In the second section, the developed numerical tool is elaborated. In the third section, numerical examples for different cases of cavity metamaterials are presented, while in the final section, the conclusions are addressed.

2 METHODS

2.1 Topological design

A metamaterial with different inner topologies containing squared, circular, elliptical or star-shaped cavities are considered (Fig. 1). In each case, the metamaterial geometry is simply generated through the knowledge of the parametric form of the cavity geometry, the number of the repetitions of each cavity to form the unit cell and the number of repetitions of the unit cell for the periodic metamaterial analyiss. The parameters defining the cavity geometry are the cavity side length and radius for square and circular patterns, respectively (Fig. 2). In the case of elliptical cavities, the parameters are the two ellipse radii and the orientation angle. Finally, in the case of star-shaped cavities, the shape is generated by intersecting two ellipses with the same dimension. Therefore, the parameters are the same as the case of the elliptical cavity; the radii α, β and the orientation angle φ. We denote the first size parameter (radius for circle, side length for square, large ellipse radius) with α. In the case of elliptical and star-shaped cavity the second size parameter is denoted with β and is related with α, given a Volume fraction V_f. Also, the parameter that deals with the orientation angle is denoted with φ. The parameters, as well as the Volume fraction relations for the different cavity geometries are summarized in Table 1.

Consider each cavity to be enclosed to a cell V_0. This cell is repeated horizontal and vertically to form the unit cell (Fig. 2). Then, the formation of the metamaterial geometry is obtained by the repetition of the already formed unit cell, as shown in Fig. 2.

2.2 Boundary Element formulation of thermoelasticity

Consider the thermoelastic problem for the cavity metamaterial of Fig. 3, where Ω_m is the domain occupied with the base material with Young modulus E, Poisson ratio ν, thermal

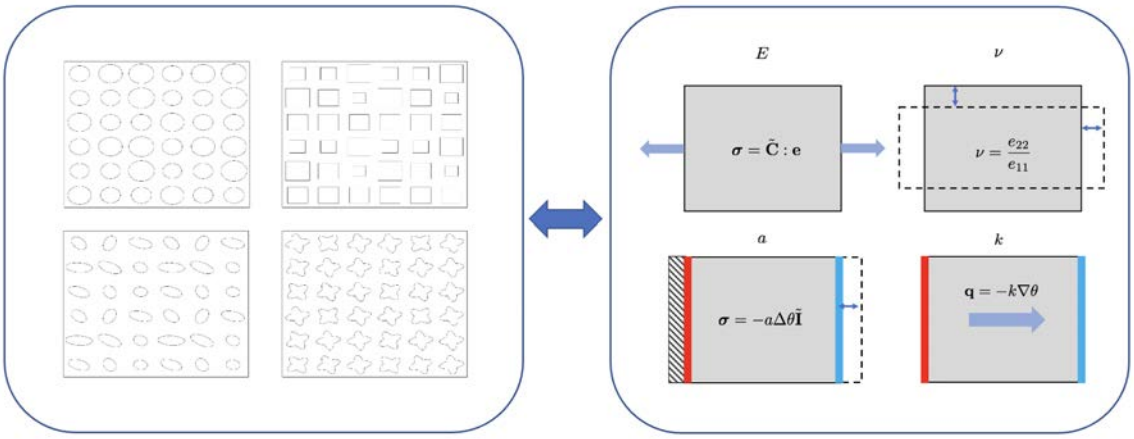

Figure 1: Cavity metamaterials and attributes

Table 1: Cavity parameters and Volume fraction relations

Cavity type	Parameters	Volume fraction relation
Square	α	$V_f = \frac{\sum_{i=1} \alpha_i^2}{l^2}$
Circular	α	$V_f = \frac{\sum_{i=1} \pi\alpha_i^2}{l^2}$
Elliptical	α, β, φ	$V_f = \frac{\sum_{i=1} \pi\alpha_i\beta_i}{l^2}$
Star-shaped	α, β, φ	$V_f = 4\frac{1}{l^2}\sum_{i=1}\left(\int_0^{x_0} \alpha_i\sqrt{1-\frac{x^2}{\beta_i^2}}dx + \int_{x_0}^{\alpha_i} \beta_i\sqrt{1-\frac{x^2}{\alpha_i^2}}dx\right)$

conductivity k and thermal expansion coefficient a, while $\Omega_c = \bigcup_i \Omega_i = \Omega \setminus \Omega_m$ denotes the domain covered by the cavities. Assuming homogeneous and isotropic linear behavior for the base material Ω_m and absence of distributed body elastic and thermal loads, the temperature φ and displacement vector $\mathbf{u}$ satisfy the following Partial Differential Equations [10]:

$$\begin{gathered} \Delta\theta = 0 \\ \mu\Delta\mathbf{u} + (\lambda+\mu)\nabla\nabla\cdot\mathbf{u} - a(3\lambda+2\mu)\nabla\theta = \mathbf{0}, \ \mathbf{r} \in \Omega_m \end{gathered} \tag{1}$$

where

$$\lambda = \frac{E\nu}{(1+\nu)(1-2\nu)}, \ \mu \ = \frac{E}{2(1+\nu)} \tag{2}$$

and boundary conditions:

$$\left.\begin{matrix} k\partial_n\theta = 0 \\ \mathbf{t} = \mathbf{0} \end{matrix}\right\}, \ \mathbf{r} \in \Gamma_N, \ \left.\begin{matrix} \theta = \theta_L \\ u_1 = 0 \end{matrix}\right\}, \ \mathbf{r} \in \Gamma_L, \ \left.\begin{matrix} \theta = \theta_R \\ u_1 = u_0 \end{matrix}\right\}, \ \mathbf{r} \in \Gamma_R, \ u_2 = 0, \ \mathbf{r} = \mathbf{0} \tag{3}$$

where ∇ denotes the nabla operator, $\Delta = \nabla\cdot\nabla$ denotes the Laplace operator and $\partial_n = \frac{\partial}{\partial_n} = \mathbf{n}\cdot\nabla$ is the normal to surface derivative. The vector $\mathbf{t} = \lambda(\nabla\cdot\mathbf{u})\mathbf{n} + 2\mu\mathbf{n}\cdot\nabla\mathbf{u} + \mu\mathbf{n}\times\nabla\times\mathbf{u}$ is the

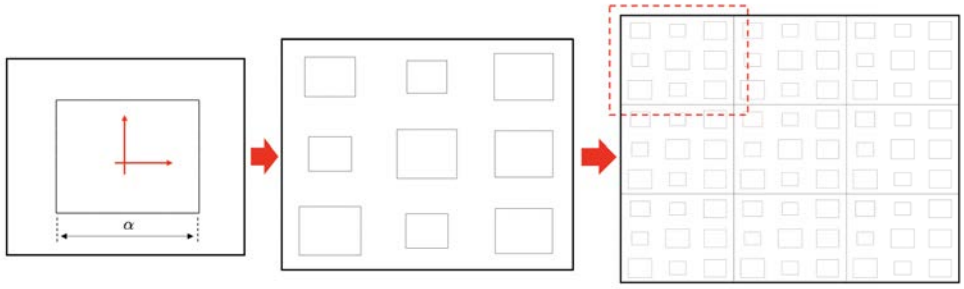

(a)

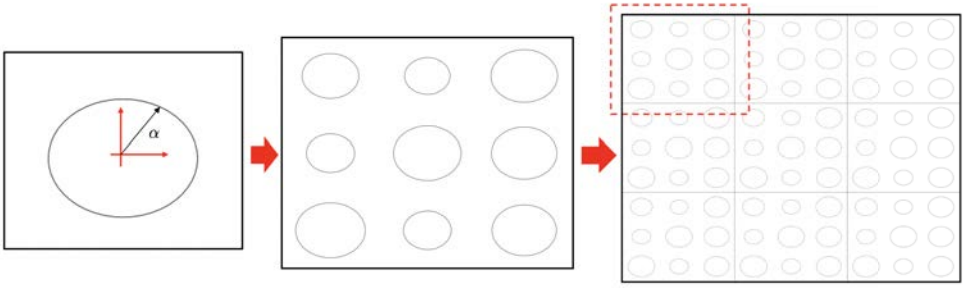

(b)

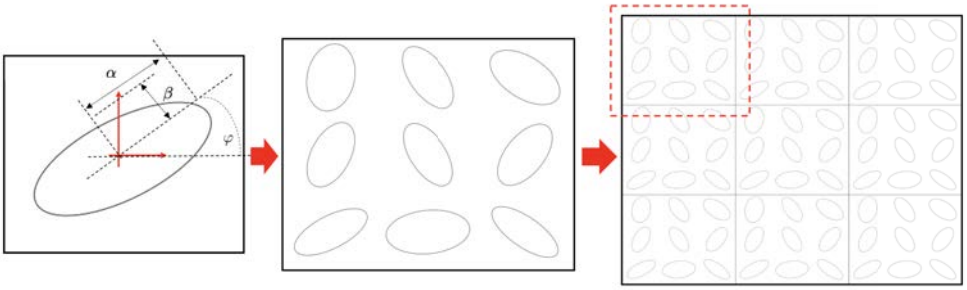

(c)

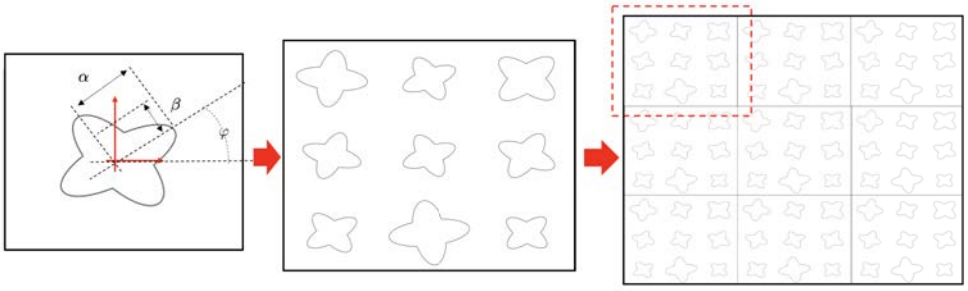

(d)

Figure 2: Formation of the cavity metamaterial. (a) square cavities, (b) circular cavities, (c) elliptical cavities, (d) star-shaped cavities

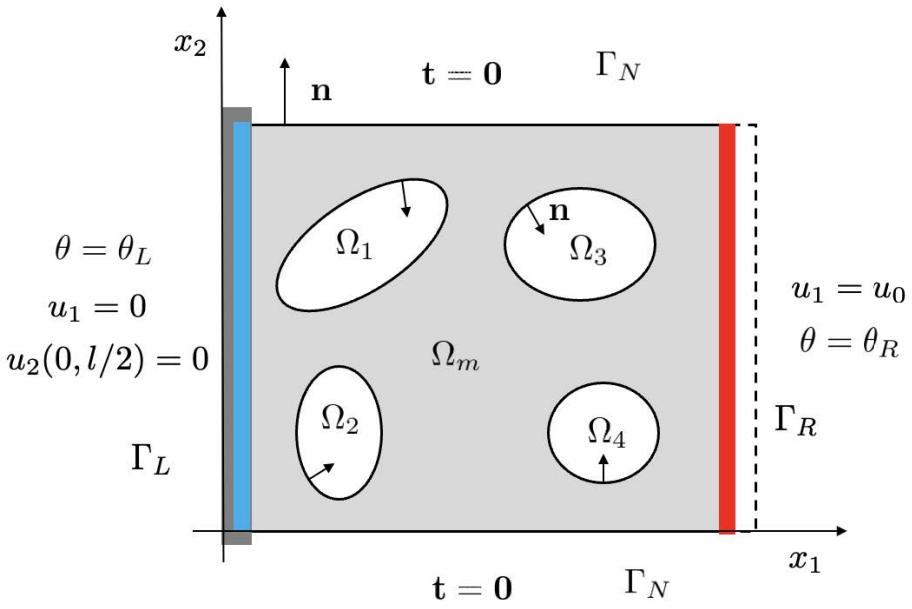

Figure 3: The boundary value problem of static thermoelasticity

surface traction, while $u_1 = \hat{\mathbf{x}}_1 \cdot \mathbf{u}$ and $u_2 = \hat{\mathbf{x}}_2 \cdot \mathbf{u}$ denote the components of the displacement vector in each direction, $\hat{\mathbf{x}}_1, \hat{\mathbf{x}}_2$ being the Cartesian unit basis vectors.

The system of Boundary Integral Equations for linear thermoelasticity, according to [11], has the following form:

$$\mathcal{T}(\mathbf{r}') = \frac{1}{2}\theta(\mathbf{r}') + \int_\Gamma \partial_n G(\mathbf{r}, \mathbf{r}')\theta(\mathbf{r}) d\Gamma - \int_\Gamma G(\mathbf{r}, \mathbf{r}')\partial_n \theta(\mathbf{r}) d\Gamma = 0 \tag{4}$$

$$\begin{aligned} \mathcal{U}(\mathbf{r}') = \frac{1}{2}\mathbf{u}(\mathbf{r}') + \int_\Gamma \left[\tilde{\mathbf{T}}(\mathbf{r}, \mathbf{r}') \cdot \mathbf{u}(\mathbf{r}) - \mathbf{P}(\mathbf{r}, \mathbf{r}')\theta(\mathbf{r})\right] d\Gamma - \\ \int_\Gamma \left[\tilde{\mathbf{U}}(\mathbf{r}, \mathbf{r}') \cdot \mathbf{t}(\mathbf{r}) + \mathbf{Q}(\mathbf{r}, \mathbf{r}')\partial_n \theta(\mathbf{r})\right] d\Gamma = \mathbf{0} \end{aligned} \tag{5}$$

where $\mathbf{r}$, $\mathbf{r}'$ denote the source and field points, respectively, while the integral kernels $G(\mathbf{r}, \mathbf{r}')$, $\partial_n G(\mathbf{r}, \mathbf{r}')$, $\tilde{\mathbf{U}}(\mathbf{r}, \mathbf{r}')$,$\tilde{\mathbf{T}}(\mathbf{r}, \mathbf{r}')$,$\mathbf{P}(\mathbf{r}, \mathbf{r}')$,$\mathbf{Q}(\mathbf{r}, \mathbf{r}')$ are provided in [11].

A standard Galerkin formulation is followed, multiplying the first and the second integral equation with a scalar weight function Ψ^k and a vector weight function $\mathbf{N}^k$, respectively, and integrating over the boundary Γ with respect to the coordinates of $\mathbf{r}'$ ([12]), i.e:

$$\begin{aligned} \int_\Gamma \Psi^k(\mathbf{r}')\mathcal{T}(\mathbf{r}') d\Gamma' = 0 \\ \int_\Gamma \mathbf{N}^k(\mathbf{r}') \cdot \mathcal{U}(\mathbf{r}') d\Gamma' = 0 \end{aligned} \tag{6}$$

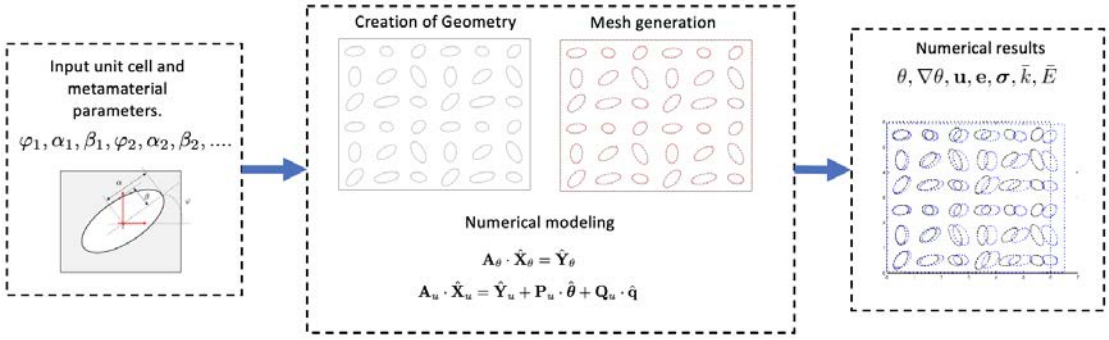

Figure 4: The proposed numerical tool

Implementing the Galerkin Boundary Element procedure using quadratic boundary elements, we obtain the discretized equations, written in matrix form:

$$\begin{aligned} \mathbf{H}_u \cdot \hat{\mathbf{u}} &= \mathbf{G}_u \cdot \hat{\mathbf{t}} + \mathbf{P}_u \cdot \hat{\boldsymbol{\theta}} + \mathbf{Q}_u \cdot \hat{\mathbf{q}} \\ \mathbf{H}_\theta \cdot \hat{\boldsymbol{\theta}} &= \mathbf{G}_\theta \cdot \hat{\mathbf{q}} \end{aligned} \tag{7}$$

Applying the boundary conditions (3) in (7) and rearranging to separate known from unknown boundary nodal values, the matrix equations (7) results in the equations

$$\begin{aligned} \mathbf{A}_\theta \cdot \hat{\mathbf{X}}_\theta &= \hat{\mathbf{Y}}_\theta \\ \mathbf{A}_u \cdot \hat{\mathbf{X}}_u &= \hat{\mathbf{Y}}_u + \mathbf{P}_u \cdot \hat{\boldsymbol{\theta}} + \mathbf{Q}_u \cdot \hat{\mathbf{q}} \end{aligned} \tag{8}$$

with $\hat{\mathbf{X}}_\theta$ and $\hat{\mathbf{X}}_u$ being the vectors containing all the unknown nodal values regarding the heat conduction and elasticity, respectively.

2.3 Effective property computation

Based on the Boundary Element Method described in the previous subsection, the numerical implementation of the method is developed [13]. This analysis process is described briefly in the flow chart of Fig. 4. The model takes as input the cavity geometric parameters. The orientation angle φ takes values in the interval $[0, \pi)$. For the size parameters α, β we have: $\alpha, \beta \in (0, l_f - \epsilon]$, with ϵ being a small enough number that ensures that each cavity will not intersect with a neighboring cavity and l_f denotes the size of the cell V_0. With these parameters as input arguments, the model creates the boundary element mesh and simulates the thermoelastic behaviour of the metamaterial, solving the matrix equations (8). Then, the effective properties, as well as the field values are calculated and provided as outputs. In order to compute the effective properties $\bar{E}_x$, $\bar{E}_y$, $\bar{k}_x$, flux field calculations on the boundary are required. The calculation of the effective conductivity is obtained by:

$$\bar{k}_x = \frac{Ql}{Area(\Gamma_R)\Delta\theta} \tag{9}$$

Table 2: Calculated effective properties

	Uniform			Non-uniform		
	$\bar{E}_x$	$\bar{E}_y$	$\bar{k}_x$	$\bar{E}_x$	$\bar{E}_y$	$\bar{k}_y$
Square	0.507	0.507	0.511086	0.497	0.499	0.508
Circular	0.516	0.516	0.54	0.504	0.507	0.537
Elliptical	0.635	0.347	0.626	0.393	0.487	0.452
Star-shaped	0.37	0.37	0.439	0.537	0.559	0.596

where:

$$Q = -\int_{\Gamma_R} k\partial_n \theta d\Gamma \tag{10}$$

Following the same way, the effective Young Modulus is given by:

$$\bar{E}_x = \frac{Fl}{Area(\Gamma_R)\Delta u} \tag{11}$$

where:

$$F = \int_{\Gamma_R} \mathbf{n} \cdot \mathbf{t} d\Gamma \tag{12}$$

The thermal flux and the surface traction fields in the integrals of (10) and (12) are approximated with the nodal values acquired from the solution of (8), then a numerical integration procedure over the boundary Γ_R is applied to compute Q and F.

3 NUMERICAL RESULTS

In this section, the numerical model is employed to calculate the effective properties for each metamaterial topology above introduced. For all cases, unit-cells containing 3x3 cavities of different volumetric contents (random cavity dimensions and orientation angles), as well as uniform cavity volumes are employed. In both cases, the dimensions and orientation angles of the cavities satisfy the constraint of a total volume fraction of 30%. In the case of the uniform cavity dimensions, the orientation angle is set to zero. The boundary conditions described in Fig. 3, as well as Eq. 3 are employed for all the analyses.

Figure 5 depicts the undeformed metamaterial topologies along with their deformed shape, while Table 2 presents the computed effective properties for each case. It should be mentioned that the effective properties are normalized with respect to the properties of the base material. In the case of uniform cavity distributions, the Young's moduli in the horizontal and vertical direction are equal, validating the consistency of the computations. Moreover, in the case of the uniform elliptical cavities the modulus $\bar{E}_x$ is much larger than $\bar{E}_y$, as the effect of the orientation angle plays significant role. The same applies to the horizontal effective thermal conductivity $\bar{k}_x$, where in the case of uniform elliptical cavities, the largest value is obtained compared to all other cavity topologies.

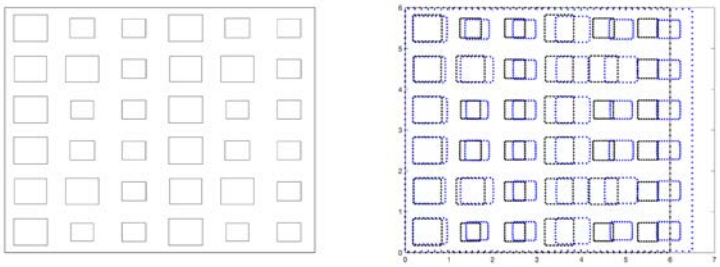

(a)

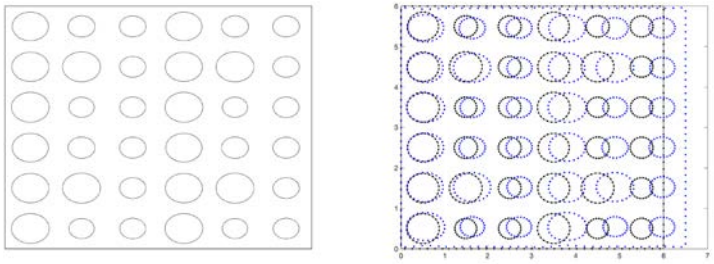

(b)

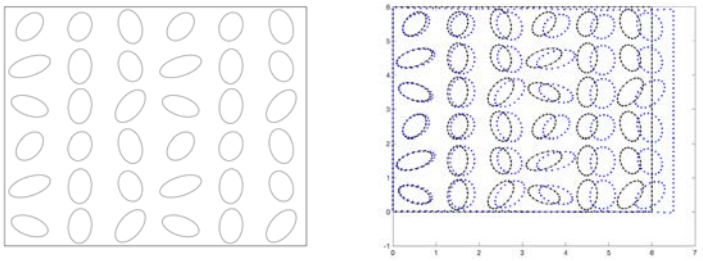

(c)

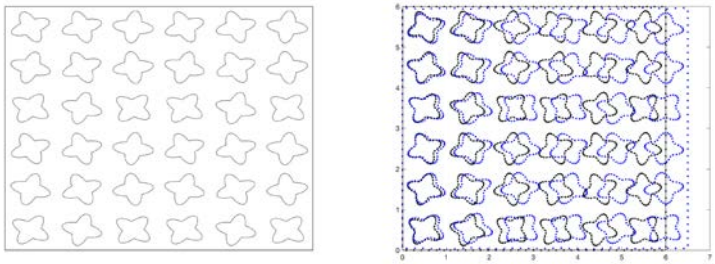

(d)

Figure 5: Geometry and deformed shape of the metamaterial with (a) square cavities, (b) circular cavities, (c) elliptical cavities, (d) star-shaped cavities

4 CONCLUSIONS

In the present work, a numerical model for the design of metamaterials with inner cavities has been elaborated. The model has been based on the Galerkin Boundary Element Method and offers the advantage of accurate thermal flux and surface traction evaluation on the geometry boundary, as of the very formulation of the Boundary Element Method, allowing for high accuracy effective property computation. The model requires solely the discretization of the surfaces allowing for the direct generation of the target topologies, without the need for a mesh generator. The elaborated model has been employed in the computation of the effective thermoelastic attributes of different metamaterial topologies. The current analysis can be used not only for the single step, forward computation of the effective properties of parametrically defined metamaterial topologies, but it can be handily extended to include optimization techniques in the inverse determination of the inner cavity form pattern for given thermal conductivity or elastic property objectives.

REFERENCES

[1] T. D. Ngo, A. Kashani, G. Imbalzano, K. T. Q. Nguyen, and D. Hui, "Additive manufacturing (3D printing): A review of materials, methods, applications and challenges," *Composites Part B: Engineering*, vol. 143, pp. 172–196, 2018. [Online]. Available: https://www.sciencedirect.com/science/article/pii/S1359836817342944

[2] M. Askari, D. A. Hutchins, P. J. Thomas, L. Astolfi, R. L. Watson, M. Abdi, M. Ricci, S. Laureti, L. Nie, S. Freear, R. Wildman, C. Tuck, M. Clarke, E. Woods, and A. T. Clare, "Additive manufacturing of metamaterials: A review," *Additive Manufacturing*, vol. 36, p. 101562, 2020. [Online]. Available: https://www.sciencedirect.com/science/article/pii/S2214860420309349

[3] O. Al-Ketan, A. Singh, and N. Karathanasopoulos, "Strut and sheet metal lattices produced via am-assisted casting and powder bed fusion: A comparative study," *Additive Manufacturing Letters*, vol. 4, p. 100118, 2023. [Online]. Available: https://www.sciencedirect.com/science/article/pii/S2772369022000858

[4] W. Li, M. Xu, H.-X. Xu, X. Wang, and W. Huang, "Metamaterial Absorbers: from Tunable Surface to Structural Transformation," *Advanced Materials*, vol. n/a, no. n/a, p. 2202509. [Online]. Available: https://onlinelibrary.wiley.com/doi/abs/10.1002/adma.202202509

[5] I. M. El-Galy, B. I. Saleh, and M. H. Ahmed, "Functionally graded materials classifications and development trends from industrial point of view," *SN Applied Sciences*, vol. 1, no. 11, p. 1378, 2019. [Online]. Available: https://doi.org/10.1007/s42452-019-1413-4

[6] N. Karathanasopoulos and D. Rodopoulos, "Enhanced Cellular Materials through Multi-

scale, Variable-Section Inner Designs: Mechanical Attributes and Neural Network Modeling," *Materials*, vol. 15, 2022.

[7] L. Yang, O. Harrysson, H. West, and D. Cormier, "Mechanical properties of 3D re-entrant honeycomb auxetic structures realized via additive manufacturing," *International Journal of Solids and Structures*, vol. 69-70, pp. 475–490, 2015. [Online]. Available: https://www.sciencedirect.com/science/article/pii/S0020768315002152

[8] L. Wrobel, *The boundary element method. volume1: applications in thermo-fluids and acoustics*. England, Wiley, 2002.

[9] D. Rodopoulos, S. Atluri, and D. Polyzos, "A hybrid FPM/BEM scalar potential formulation for field calculations in nonlinear magnetostatic analysis of superconducting accelerator magnets," *Engineering Analysis with Boundary Elements*, vol. 128, pp. 118–132, 2021.

[10] M. R. Eslami, R. B. Hetnarski, J. Ignaczak, N. Noda, N. Sumi, and T. Y., *Theory of Elasticity and Thermal Stresses. Explanations, Problems and Solutions*, ser. Solids Mechanics and its Applications. Springer, 2013, vol. 197.

[11] F. M. H. Aliabadi, *The Boundary Element Method: Applications in Solids and Structures*. Wiley, 2002, vol. 2.

[12] A. Sutradhar, G. H. Paulino, and L. J. Gray, *Symmetric Galerkin Boundary Element Method*. Springer, 2008, vol. 2.

[13] MATLAB, *9.12.0.2170939 (R2022a)*. Natick, Massachusetts: The MathWorks Inc., 2022.